RSC Advances

PAPER

View Article Online
View Journal | View Issue

Cite this: *RSC Adv.*, 2024, **14**, 32021

Thermo-controlled microfluidic generation of monodisperse alginate microspheres based on external gelation†

Saray Chen, *[a] Tal Shahar [a] and Smadar Cohen[ab]

Droplet-based microfluidic systems have received much attention as promising tools for fabricating monodisperse microspheres of alginate solutions with high accuracy and reproducibility. The immediate and simple ionotropic gelation of alginate, its biocompatibility, and its tunability of mechanical properties make it a favorable hydrogel in the biomedical and tissue engineering fields. In these fields, micron-sized alginate hydrogel spheres have shown high potential as cell vehicles and drug delivery systems. Although on-chip microfluidic gelation of the produced alginate droplets is common, several challenges remain. Complicated chemical and microfabrication processes are required, and the risk of microchannel clogging is high. In the current study, we present an easy-to-use microfluidic external gelation process to produce highly spherical and monodisperse microspheres from very low-concentrated alginate-RGD solution [0.5% (w/v)]. To accomplish this, gelatin, a thermo-sensitive and inexpensive biomaterial, was incorporated into the alginate solution as a sacrificial biomaterial that mediates the off-chip external gelation of the alginate with Ca^{2+}, and avoids droplet coalescence. Utilizing the methodology mentioned above, we successfully generated monodisperse alginate microspheres (AMs) with diameters ranging from 27 μm to 46 μm, with a coefficient of variation of 0.14, from a mixture of Arg-Gly-Asp (RGD)-modified very low viscosity alginate and gelatin. These RGD-AMs were used as microcarriers for human umbilical vein endothelial cells. The described easy-to-use and cost-effective microfluidic off-chip external gelation strategy exhibits comparable advantages to on-chip external gelation and demonstrates superiority over the latter since clogging is impossible.

Received 30th September 2024
Accepted 2nd October 2024

DOI: 10.1039/d4ra07049f

rsc.li/rsc-advances

Introduction

Alginate is an anionic polysaccharide comprising two copolymers, β-D-mannuronic acid and α-L-guluronic acid, extracted from brown algae.[1] Its biocompatibility, immediate and simple ionotropic gelation, and tunability of mechanical properties make it a favored hydrogel in the biomedical field.[2,3] In tissue engineering, micron-sized alginate spheres have received much attention as an attractive vehicle for cell delivery and release of drugs and other biologically active molecules with various applications.[4–7] Alginate is biologically inert and, without modification, does not support cell adhesion.[8] Previous studies have shown that immobilizing an Arg-Gly-Asp (RGD) peptide to alginate scaffolds promotes cell adherence to the matrix.[9,10] The RGD peptide is the signaling domain derived from fibronectin and laminin, and is the most used extracellular matrix (ECM)-derived peptide for biomaterial modification in tissue engineering.[11] The shape and size of alginate hydrogels are critical to their applications.[12] For example, the surface area is crucial for controlling the kinetics of drug release. Therefore, monodisperse hydrogels with a spherical shape are required for precise control over drug dosage and sustained release.[13] A highly controlled fabrication method is essential for fabricating alginate microspheres (AMs) with the desired properties. In recent years, droplet-based microfluidic systems have gained considerable attention due to their capability to generate monodisperse small spherical droplets from alginate solutions with high reproducibility, accuracy, and throughput.[14] The production of AMs in a microfluidic system typically consists of two steps: emulsification of an aqueous alginate solution in an oil phase, followed by external/internal gelation of the generated droplets, which can be performed either on-chip or off-chip.[15]

There are several reports regarding on-chip external gelation of alginate droplets that resulted in highly-sphered and monodisperse microspheres.[16–18] The on-chip gelation process is generally preferred since it enables continuous generation of AMs with a high degree of monodispersity. However, some challenges remain in this approach. One of them is

[a]*The Avram and Stella Goldstein-Goren Department of Biotechnology Engineering, Ben-Gurion University of the Negev, Beer-Sheva 84105, Israel. E-mail: sarayha@post.bgu.ac.il*

[b]*Regenerative Medicine and Stem Cell (RMSC) Research Centre, Ben-Gurion University of the Negev, Beer-Sheva 84105, Israel*

† Electronic supplementary information (ESI) available. See DOI: https://doi.org/10.1039/d4ra07049f

microchannel clogging that occurs due to a rapid increase in viscosity in the precursor solutions during crosslinking.[19] In addition, the studies thus far conducted of on-chip alginate crosslinking suffer from complicated chemical and microfabrication processes.[20–22]

Off-chip external gelation usually occurs by collecting droplets after generation into a gelation bath containing Ca^{2+} ions. However, the alginate droplets either cannot break the oil/water interface to enter the gelation bath or are gradually crosslinked, resulting in creation of a tailed-shaped particle while passing through the interface.[23] Moreover, when lowering aqueous phase viscosity, the generated droplets tend to fuse during the flow due to interfacial tension before the gelation step in the bath.[24,25] This tendency presents a considerable obstacle to synthesizing monodisperse low-concentrated AMs by external gelation in an off-chip mode. The ability to generate AMs from this kind of solution is essential for controlling the dissolution rate of the AMs.

It is well-established that biopolymer blending is a practical and efficient method for improving the performance of biopolymers.[26] Specifically, alginate–gelatin composite gels are used in biomedical applications and tissue engineering.[27,28] These composite gels are particularly notable for their ability to offer complex functionalities, such as serving as bioinks for 3D bioprinting,[29] drug-loaded films,[30] *etc.* Gelatin is a cost-effective biomaterial that may form thermo-reversible gels below physiological temperatures.[31] In a biopolymer blend, molecular interactions and phase behavior can change significantly upon gelation. While the components may exhibit co-solubility in their liquid state, phase separation can occur when one of the biopolymers undergoes gelation.[26,29]

The current study aimed to produce micron-sized, monodispersed, and highly-sphered AMs, using very low-concentrated alginate-RGD solution [0.5% (w/v)] as an aqueous phase, by off-chip external gelation. However, microsphere generation from very low viscosity solutions can be hindered by droplet coalescence during flow. Hence, gelatin was incorporated into the alginate solution as a sacrificial biomaterial that mediated the off-chip external gelation of alginate micro-droplets with Ca^{2+} ions. This approach is based on two gelling steps: thermal gelation of gelatin in the outlet tube, which fixates droplet size and shape, thus, preventing droplet fusion; and physical crosslinking of alginate in a canola oil bath containing $CaCl_2$ nanoparticles. The described strategy presents advantages similar to on-chip external gelation and is superior since there is no possibility of clogging, and the chemical and microfabrication processes are uncomplicated. In addition, the AMs were examined as a platform for human umbilical vein endothelial cells (HUVEC) adherence.

Experimental section

Materials

Sodium alginate (VLVG, 70% guluronic acid monomer content) was obtained from FMC Biopolymers (Drammen, Norway). Alginate-RGD (Alg-RGD, 32.3 kDa) was synthesized from VLVG utilizing the aqueous carbodiimide chemistry previously described,[32] to yield a 0.2% degree of modification of uronic acid monomers by the peptide sequences. The peptide-modified alginate product was purified by dialysis (3500 Da MW cut-off) against double-distilled water for 3 days, and then lyophilized until dry. Alginate-RGD FTIR spectra confirming the presence of peptide bonds are shown in ESI Fig. S1.† Labeling of alginate by HiLyte Fluor™ 488 amine (AnaSpec, Fremont, CA) was performed according to Sapir *et al.*[9] Gelatin type B was purchased from Sigma-Merck (Rechovot, Israel). Commercial-grade canola oil was purchased from a local grocery store.

Microfluidic device fabrication

The microfluidic device with channel dimensions of 150 μm in width and 50 μm in height was fabricated using conventional photolithography and soft lithography methods. Briefly, the mold master was made by patterning SU-8 photoresist on a silicon wafer. A PDMS mixture [with a 10 : 1 ratio of base: curing agents (Sylgard 184, Dow Corning)] was poured onto the mold master, degassed, and cured for 1 h at 60 °C. After curing, the PDMS replica containing the microchannel pattern was peeled off from the master, and holes were punched in it with a 0.75 mm tissue punch (NBT). The PDMS replica was bonded to a glass microscope slide after exposure to an oxygen plasma for 20 s. To make the channels hydrophobic and prevent wetting, they were coated with Aquapel (PPG Industries, Pittsburgh, PA).

On-chip generation of Alg-RGD droplet

The microfluidic device features two inlets; one for the flow of the aqueous phase [0.5% (w/v) Alg-RGD, 0.1% and 1.7% gelatin dissolved in DDW] and one for the flow of the continuous phase (canola oil with 2% Span-80 as a surfactant). The solutions were loaded in plastic syringes, connected to the microfluidic device using Tygon® tubing [with an internal diameter of 0.2 mm (Cole-Parmer)], and injected at controlled flow rates using syringe pumps (InfusionONE Syringe Pump, Darwin Microfluidics). The generation of water-in-oil droplets occurred at a flow-focusing junction and was examined using an inverted microscope (Olympus IX70). Simultaneously, the Tygon® outlet tube was cooled on ice to a temperature below that of the gelatin's gelling temperature (T_g). Microspheres were collected in a glass vial filled with 15 mL of canola oil with $CaCl_2$ nanoparticles. To avoid uncontrolled gelatin gelation, the process was carried out in a pre-heated room at 25 °C, which is above the gelatin gelling temperature. Additionally, a Styrofoam sheet (2 cm × 2 cm) was placed between the chip glass and the ice to prevent chip cooling.

To remove the oil phase, 5 mL of 1% (w/v) $CaCl_2$ aqueous solution was added to the vial after microsphere collection. The sample was then centrifuged at 400 g for 10 min, and the oil phase was removed. The resultant microspheres were maintained in 1% $CaCl_2$ solution till use. Before use, the microspheres were rewashed with culture medium and incubated at 37 °C for 30 min.

Production of $CaCl_2$ nanoparticles

$CaCl_2$ nanoparticles in canola oil were prepared as previously described.[33] Briefly, a volume ratio of 5% of a 0.1 molal solution

of $CaCl_2$ in pure ethanol was added to canola oil containing 6% (w/w) of Span-80. The mixture was sonicated for 1 min and heated overnight at 60 °C while stirring on a magnetic stirrer for alcohol evaporation. Then, the sample was cooled to room temperature before use.

Changes in phase angle during cooling of alginate-RGD-gelatin solution

The gelling temperature of the Alg-RGD-Gel solution was measured using a controlled stress rheometer. The solution was pre-heated at 30 °C. The measuring geometry used was a 60 mm 1° steel cone. The measurement was performed at a scan rate of 0.5°C min^{-1} at a frequency of 1 Hz, with oscillating applied stress of 0.5 Pa during cooling from 30° to 3 °C. The gelling temperature was calculated, where tan (δ) became one or δ was 45°. A sharp decrease and rapid transition in the phase angle during cooling were considered as the increase in the amount of energy elastically stored in the storage modulus (G').[34]

Characterization of obtained alginate droplets and microspheres

The coefficient of variation (CV) of 40 droplets was evaluated to characterize the monodispersity of the generated droplets. A digital camera (Olympus DF72) captured bright-field images of the droplets and microspheres. ImageJ (NIH, USA) analysis software was used to analyze the captured images and to evaluate the CV, droplet and microsphere diameter D, and roundness R, according to the following equations:

$$D = 2\sqrt{A/\pi},\ R = 4\pi A/P^2$$

where A is the projected area, and P is the perimeter of the droplet/microsphere. For ellipsoid droplets in the channel, diameter D was calculated according to $D = \sqrt[3]{C^2B}$, where B is the major axis of the ellipsoid, and C is the minor axis. As we assume it is a body rotation with respect to the long axis (major axis), the other two axes are equal. The volume (V_e) of such an ellipsoid is $V_e = 4\pi A^2 B/3$, and the volume (V_S) of a sphere with a diameter D is $V_S = \pi D^2/3$. Therefore, the equivalent diameter of a sphere with the same volume as that of the ellipsoid is $D = \sqrt[3]{C^2B}$.

Scanning electron microscopy (SEM)

Alg-RGD-Gel/Alg-RGD microspheres were dried overnight at room temperature (~25 °C) and then sputter-coated with gold. The imaging was performed using a Gemini SEM (Zeiss) microscope at an accelerating voltage of 5 kV under a high vacuum. The measurements were done at the Ilse Katz Institute for Nanoscale Science and Technology at Ben-Gurion University of the Negev in Beer Sheva, Israel.

Cryo SEM

Samples of the Alg-RGD-Gel/Alg-RGD microspheres were placed and sandwiched between two aluminum discs (3 mm in diameter, each 25 μm thick), and cryo-immobilized in a high-pressure freezing device (EM ICE, Leica). The frozen samples were then mounted on a holder under liquid nitrogen in a specialized loading station (EM VCM, Leica) and transferred under cryogenic conditions (EM VCT500, Leica) to a sample preparation freeze fracture device (EM ACE900, Leica). In that device, the samples were fractured by a rapid stroke of a cryogenically cooled knife, exposing the inner part of the sandwiched discs. After fracturing, the samples were etched at −100 °C for 5 min to sublime ice from the sample surface and coated with 3 nm of carbon. Samples were imaged in a Gemini SEM (Zeiss) by a secondary electron in-lens detector while maintaining an operating temperature of −120 °C. The measurements were performed at the Ilse Katz Institute for Nanoscale Science and Technology at Ben-Gurion University of the Negev in Beer Sheva, Israel.

Cell culture

Primary human umbilical vein endothelial cells (HUVECs) (Lonza) were grown in complete endothelial growth medium (EGM-2), supplemented with a Bullet kit® (Lonza) containing fetal bovine serum, nutrients, and hormones. The endothelial cells were grown in a 5% CO_2 incubator at 37 °C.

To measure the HUVEC attachment onto the RGD-AMs, HUVECs (passage 4–5) were trypsinized, counted using a Trypan blue exclusion assay, and mixed with RGD-AMs at a ratio of 5, 25, and 50 cells per RGD-AM in culture medium. The cell/RGD-AM mixture was cultured in suspension under gentle agitation in a 5% CO_2 incubator at 37 °C for up to 3 h.

Flow cytometry

After 1 h or 3 h of incubation, the HUVEC with RGD-AM samples in suspension were fixated using a Foxp3/Transcription Factor Staining Buffer Set (eBioscience, San Diego, CA) according to the manufacturer's instructions. Then cell nuclei were stained with propidium iodide (PI) (Thermo Fisher Scientific), according to the manufacturer's instructions. A flow cytometry analysis was performed using NovoCyte NovoSampler Pro (Acea Biosciences, Santa Clara, CA, USA), utilizing FlowJo™ software (BD Life Sciences, Franklin Lakes, NJ, USA). Sample-only cells and only RGD-AMs were measured as negative controls. The cell-populated RGD-AM percentage was calculated by dividing the PI-positive events of the RGD-AMs by the total RGD-AM events per sample.

Imaging of HUVEC-seeded RGD-AMs

For cell visualization, after 3 h of incubation, HUVEC-seeded AF488-RGD-AMs were fixated using 4% formaldehyde and stained with Alexa Fluor™ 594 Phalloidin (Thermo Fisher Scientific), according to the manufacturer's instructions. Cell nuclei were stained with NucBlue™ Live ReadyProbes™ Reagent (Hoechst 33342) (Thermo Fisher Scientific). Then images were taken using a confocal microscope (LSCM).

Statistical analysis

Results are presented as mean ± SEM. A statistical analysis was performed using a two-tailed, unpaired Student's t-test. The

statistical significance was established at $p < 0.05$. ****$p < 0.0001$.

Results and discussion

Generation of alginate-RGD droplets in a microfluidic device with a flow-focusing geometry

The current study presents a novel off-chip external gelation method for fabricating monodispersed alginate microspheres. Use of a flow-focusing microfluidic device is one of the most widely used methods for monodispersed droplet formation.[35] When two immiscible fluids flow in the device, counter-balancing viscous stress and interfacial tension between the phases leads to the formation of droplets. The droplet generation frequency and diameter can be adjusted by varying the flow rates. As shown in Fig. 1, smaller droplets were obtained by increasing the continuous phase flow rate.

External gelation of alginate-RGD microspheres (RGD-AMs)

The generation of RGD-AMs with the microfluidic device was performed in two steps: production of alginate droplets followed by droplet gelation. When using a relatively low concentration [0.5% (w/v)] and low viscosity alginate (VLVG)-RGD as a dispersed phase, monodisperse alginate droplets with diameters ranging from 31 to 48 μm, with a CV of 0.09, were successfully generated at the cross-section. However, collecting the generated droplets in a $CaCl_2$ aqueous gelation bath encourages droplet fusion.[23] Because of the minimal density difference between the alginate droplets and the $CaCl_2$ solution, droplets accumulate at the oil/water interface in the bath and fuse. As shown in Fig. 2, to avoid this problem, canola oil containing $CaCl_2$ nanoparticles was used as a gelation bath instead of the aqueous $CaCl_2$ solution. The $CaCl_2$ nanoparticle's mean radius was 4.94 ± 1.46 nm, as measured by DLS (ESI Fig. S2†). In this manner, crosslinking of the alginate droplets occurs directly at the oil/droplet interface in the collecting bath. However, rapid droplet fusion was also observed within the outlet tube, resulting in polydisperse alginate microparticles with diameters ranging from 23 to 242 μm and with a CV of 1.33.

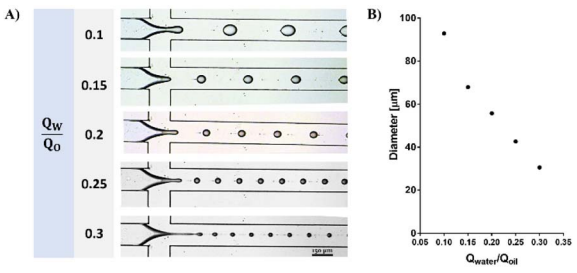

Fig. 1 Effect of the flow rate of the continuous phase on the size of the alginate-RGD droplet. (A) Size of VLVG alginate-RGD droplets controlled by fixating the inner aqueous phase flow rate (Q_w) at 1 μL min^{-1} and altering the continuous phase [Q_o, canola oil +2% (v/v) span80] flow rate. (B) Quantitative representation of droplet size as a function of flow rates. ImageJ analysis software was used to analyze droplet diameter D. Data are presented as mean ± SEM.

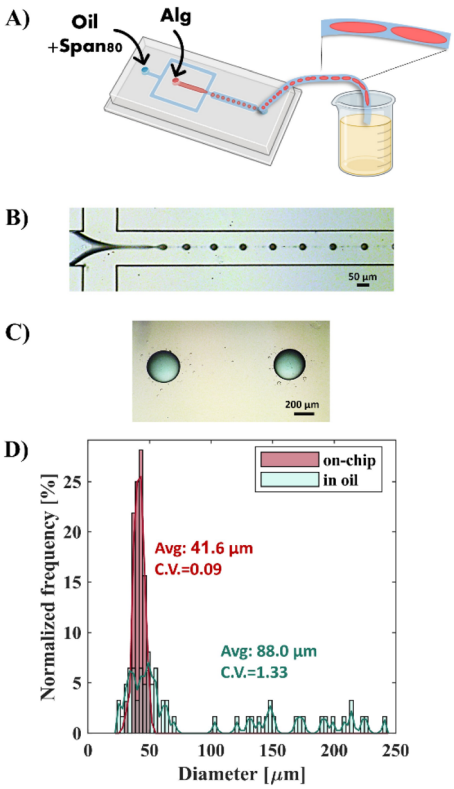

Fig. 2 Off-chip external gelation of 0.5% (w/v) RGD-AMs. (A) Schematic illustration of the process. Created with BioRender.com. (B) Generation of monodispersed alginate-RGD droplets at the cross-junction (B) RGD-AMs in oil with $CaCl_2$ nanoparticles (C) Size distribution of alginate-RGD droplets at generation and RGD-AMs in oil with $CaCl_2$ nanoparticles.

Thus, these findings emphasize the importance of instant droplet gelation after droplet generation, particularly when using a low-viscosity aqueous phase.

Generation of monodisperse alginate microspheres based on external gelation, using gelatin as a sacrificial biomaterial

Gelatin is a thermal-sensitive biomaterial that is widely used in tissue engineering.[36] Because it is temperature dependent, it is potentially an ideal candidate for use as a sacrificial biomaterial.

In the current study, based on this property, gelatin was incorporated into the alginate solution as a sacrificial biomaterial. It mediated the off-chip external gelation of the alginate-RGD droplets with $CaCl_2$ due to its capability to gel instantly when exiting from the chip at a temperature below its gelling temperature (T_g).

Specifically, as described in Fig. 3, the gelatin was used at a concentration at which it liquefies above room temperature and reversibly solidifies on ice [1.7% (w/v)]. Alginate-RGD-gelatin (Alg-RGD-Gel) monodisperse droplets were generated at a simple flow-focusing cross-junction of the microfluidic device at room temperature. Simultaneously, a Tygon outlet tube was cooled on ice to a temperature below the gelatin's T_g. This step enabled thermal gelation of the droplets, which

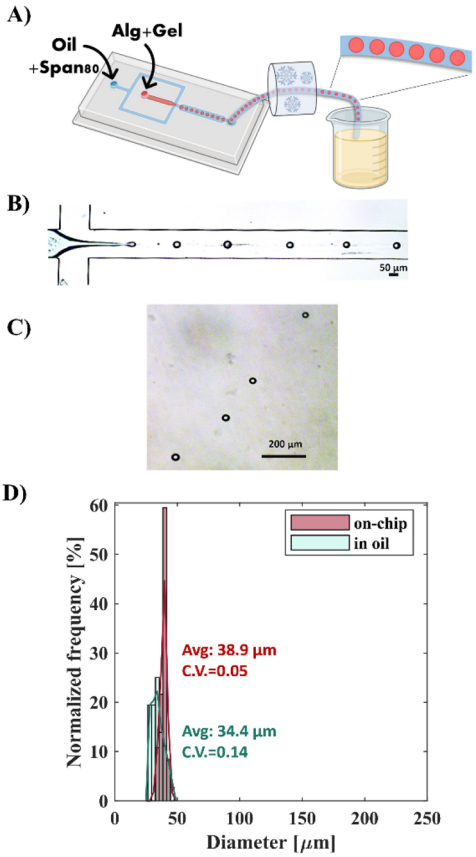

Fig. 3 Off-chip external gelation of 0.5% (w/v) alginate-RGD-1.7% gelatin microspheres. (A) Schematic illustration of the process. Created with BioRender.com. (B) Generation of monodispersed Alg-RGD-Gel droplets at the cross-junction (C) Alg-RGD-Gel microspheres in oil with $CaCl_2$ nanoparticles (D) Size distribution of Alg-RGD-Gel droplets at generation and Alg-RGD-Gel monodisperse microspheres in oil with $CaCl_2$ nanoparticles.

fixated their size and shape, thus, preventing droplet fusion. Subsequently, the gelled droplets were collected into a canola oil bath containing $CaCl_2$ nanoparticles, which resulted in ionic crosslinking of the alginate. This approach facilitated easy collection of the monodisperse Alg-RGD-Gel microspheres, with diameters ranging from 32 to 42 μm and a CV of 0.05, in oil with $CaCl_2$ nanoparticles. This diameter range is similar to that of the alginate droplets that were visualized at generation at the cross-junction. The droplet diameter at generation ranged from 27 to 46 μm, with a CV of 0.14.

To determine the gelling temperature of the Alg-RGD-Gel solution and to better understand the gelling conditions, changes in the phase angle during the cooling of the solution were measured. As seen by the sharp decrease and rapid transition in the phase angle during cooling in Fig. 4A, the gelling temperature was 19.6 °C.

Notably, the gelatin addition to the alginate-RGD solution increased its viscosity, and slightly prevented the rapid fusion of droplets within the outlet tube, regardless of temperature (see the solution viscosities in Fig. S3 in the ESI†). Nevertheless, at room temperature (RT), without cooling the tube, the droplets tended to fuse, resulting in polydisperse low-spherical particles which could be seen with the naked eye due to their size (Fig. 4B and C). In contrast, monodisperse Alg-RGD-Gel microspheres were collected after cooling and observed as a trail within the collection bath (Fig. 4D and E). Moreover, the thermal gelation of gelatin is crucial for achieving highly-sphered microparticles (Fig. 4F). Additionally, although the gelatin crosslinking, immediate crosslinking of the alginate within the collection bath is crucial for achieving monodisperse Alg-RGD-Gel microspheres. This is because collecting the gelled microspheres after cooling in canola oil with 2% span80 and without $CaCl_2$ resulted in monodisperse gelatin microspheres enclosed by large polydisperse alginate-RGD droplets, as shown in Fig. 4G. This indicates that the formed gelatin network does not trap all the uncrosslinked alginate chains.

Alg-RGD-Gel microsphere characterization

The results of a SEM analysis (Fig. 5A and B) revealed undulations and folds on the surface of the dried spheres. When performing a CryoSEM analysis, which allowed wet samples to be analyzed, these undulations were smoother (Fig. 5C). The accumulation of $CaCl_2$ nanoparticles, as observed by optical microscope on the surface of bigger AMs, without gelatin, in the collection bath (Fig. 5D), suggests that the nonuniform distribution of the $CaCl_2$ nanoparticle caused the formation of the obtained undulations. Moreover, the CryoSEM analysis uncovered nanopore cross-sections of the microspheres (Fig. 5E). As mentioned above, the current approach utilizes gelatin as a sacrificial biomaterial. Therefore, after alginate crosslinking in the collection bath and washing with $CaCl_2$ solution to remove the oil phase, the gelatin was supposed to be liquid and dissolved away from the Alg-RGD-Gel microspheres by incubation at 37 °C. Notably, gelatin is biocompatible, biodegradable, and does not produce harmful byproducts upon enzymatic degradation.[37] Hence, any gelatin residues, if present, would not interfere with cell growth and adherence nor limit the AM application for tissue engineering. Indeed, the CryoSEM analysis of the RGD-AMs post-incubation at 37 °C revealed a newly formed hollow core (Fig. 5E and F). This change, which occurred upon temperature elevation, may be associated with biopolymer blend reorganization and gelatin dissolution following its liquefaction [of note, gelatin constitutes most of the AM, 1.7% (w/v) compared to alginate, that is 0.5% (w/v)].

Moreover, the formation of the hollow core could result from a phase separation triggered by the temperature quench. The gelatin undergoes coil to helix transition below its gelling temperature,[38] and this may drive the phase separation of the blend components. It has been suggested that the main driving force toward such a phase separation is the loss in entropy due to the progressive increase in the effective molecular mass of the gelled component, decreasing the entropy of mixing.[29] Furthermore, the agglomeration of gelatin microspheres observed in the collection bath when alginate crosslinking was not applied (Fig. 4D) supports the assumption for phase separation. Hence, it is likely that the inner core of the microspheres mainly contained solid gelatin, which liquefied at 37 °C and

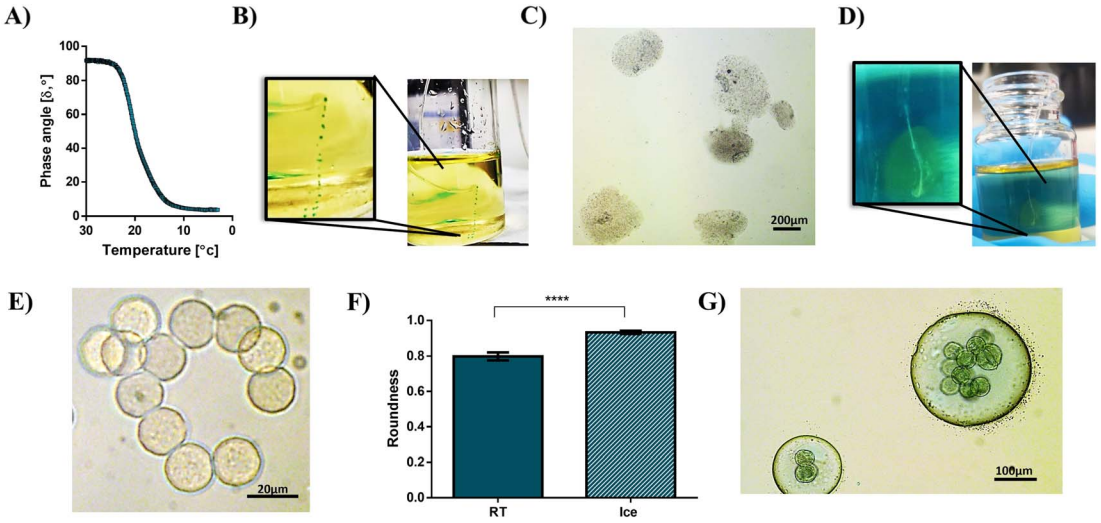

Fig. 4 Gelation of alginate-RGD-gelatin droplets. (A) Changes in the phase angle during cooling of the alginate-RGD-gelatin solution (B) Alg-RGD-Gel microspheres were collected in a canola oil bath containing $CaCl_2$ nanoparticles at room temperature, and (C) the resulting polydisperse and low-sphered microspheres as observed in an aqueous solution. (D) Pre-cooled Alg-RGD-Gel microspheres were collected in a canola oil bath containing $CaCl_2$ nanoparticles, and (E) the resulting monodisperse and highly-sphered microspheres as observed in an aqueous solution. (F) Quantitative assessment of microcarrier roundness. Data were analyzed using a two-tailed Student's *t*-test and are presented as mean ± SEM. ****$p < 0.0001$. (G) Monodisperse gelatin microspheres enclosed by larger and polydisperse alginate-RGD droplets obtained when collecting Alg-RGD-Gel microspheres, after cooling, in oil +2% (v/v) span80 without $CaCl_2$.

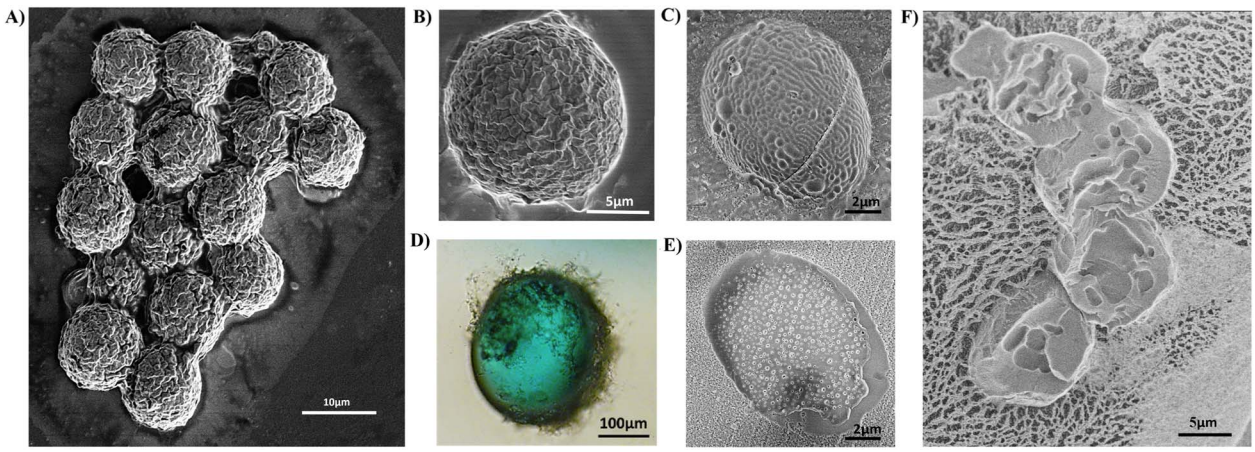

Fig. 5 (A) and (B) SEM photographs of Alg-RGD-gel microspheres. (C) CryoSEM photographs of Alg-RGD-Gel microspheres. (D) RGD-AMs (without gelatin) surrounded by $CaCl_2$ nanoparticles in a canola oil bath containing $CaCl_2$ nanoparticles, as observed by optical microscope. (E) CryoSEM photographs of Alg-RGD-Gel microsphere cross-section. (F) CryoSEM photographs of Alg-RGD microsphere cross-section after gelatin liquefaction.

dissolved away, resulting in a hollow core. Notably, the phase behaviour of biopolymer mixtures which is influenced by several factors, including biopolymer concentration, mixing ratio, temperature, pH, and ionic strength[26] could be avoided if needed, by manipulating these parameters.

RGD-AMs as microcarriers for human umbilical vein endothelial cells (HUVECs)

Using flow cytometry analysis, we measured the attachment kinetics of HUVECs onto the RGD-AMs. First, the HUVECs were seeded on the RGD-AMs at 5, 25, and 50 cells per RGD-AM. Next, the samples were fixated and stained with the nucleic acid dye propidium iodide (PI) after 1 h and 3 h in culture to elucidate a percentage of cell-populated RGD-AMs by flow cytometry analysis. Each cell-populated RGD-AM's fluorescent intensity of PI is proportional to the DNA amount, namely, the cell number attached to its surface.

After 1 h of cell incubation, the samples yielded 8.7 ± 6.0, 21.6 ± 2.9, and 29.8 ± 8.9 percent of PI-positive RGD-AMs in a seeding ratio of 5, 25, and 50 cells per RGD-AM, respectively. After 3 h of incubation, these percentages increased to 10.9 ± 5.1, 48.9 ± 4.2, and 81.8 ± 2.7 for a seeding ratio of 5, 25, and 50 cells per RGD-AM, respectively (Fig. 6A). These measurements

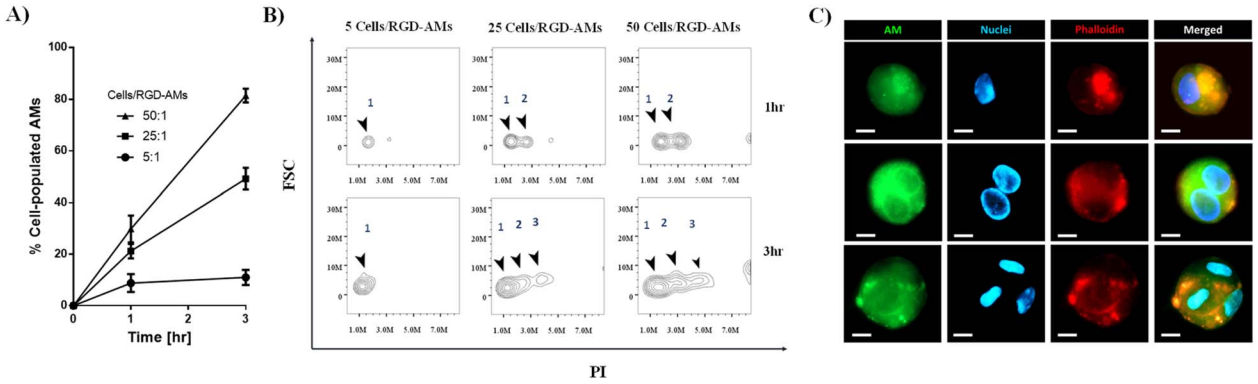

Fig. 6 Attachment of HUVECs onto AMs. (A) Attachment kinetics of HUVECs onto AMs after 1 and 3 hours of incubation. Data are presented as mean ± SEM. (B) Flow cytometry analysis of the sub-population of PI-positive AMs with different PI fluorescent intensities, proportional to the nuclei (DNA) amount on AM (1 up to 3 nuclei). (C) Maximum intensity projection of confocal images of HUVECs seeded on AMs, in a ratio of 50 cells per microcarrier. Incubation of 3 hours yielded 1–3 cells per microcarrier. Scale bar: 10 μm.

indicate that a seeding ratio of 50 cells per RGD-AM results in a satisfactory yield in 3 h. Moreover, focusing only on the PI-positive RGD-AM population, the linear scale of PI fluorescence intensity reveals sub-populations with different fluorescent intensities (Fig. 6C). Each sub-population represents RGD-AMs with a gradually increasing number of cells attached, from one cell (leftmost population) corresponding to one cell/RGD-AM to three cells (rightmost population). Notably, a seeding ratio of 50 cells per RGD-AM, after 1 h of incubation, yielded only two sub-populations compared to three sub-populations after 3 h, indicating that not only is the cell/RGD-AM ratio important, but that the incubation time is also a crucial factor. These findings are in agreement with the fact that one to three cells were observed on the RGD-AMs in the maximum intensity projection of confocal images of the HUVECs seeded on the RGD-AMs at a ratio of 50 cells per microcarrier that were incubated for 3 h. Hence, these results indicate that the generated RGD-AMs can serve as a microcarrier system for cells.

Conclusion

In the current study, microfluidic generation of alginate-RGD microspheres using an external gelation method was accomplished by employing gelatin as a sacrificial biomaterial within the alginate working solution. Gelatin mediates the off-chip external gelation of the aqueous droplets and enables the utilization of a microfluidic device with one-cross-junction flow-focusing geometry, an elementary geometry, for the generation of highly spherical and monodisperse alginate-RGD microspheres. Furthermore, by utilizing this approach, we generated monodispersed alginate-RGD microspheres even from very low-viscosity alginate solutions. The thermal gelation of the droplets within the outlet tube fixated their size and shape, thus, preventing droplet fusion during their flow in the tube. It should be noted that the cooling rate was not monitored, and future research may shed more light on this process. Next, the alginate in the Alg-RGD-Gel microspheres crosslinked by Ca^{2+} in a collection bath of canola oil containing $CaCl_2$ nanoparticles and eventually, the gelatin liquefied and dissolved away while incubating the microspheres at 37 °C. Collection of Alg-RGD-Gel into this bath at room temperature resulted in polydisperse and non-spherical alginate microspheres, emphasizing that it was not the slight increase in the viscosity of the working solution owing to the gelatin addition, but the gelation of the gelatin instantly in the chip outlet tube that enabled a satisfying product to result. A CryoSEM analysis of the RGD-AMs after incubation at 37 °C, in which the gelatin liquefied and dissolved away, revealed a hollow core, probably owing to alginate–gelatin phase separation and gelatin dissolving away from the microspheres. These AMs are suitable to use as a platform for various applications such as a delivery system of drugs,[39] cytokines,[40] cells,[41] and more. In the current study, we successfully used the RGD-AMs generated by the above-mentioned approach as a microcarrier system for HUVECs. The cell seeding ratio per RGD-AMs was examined by flow cytometry at two time-points post-cell seeding. Cell attachment to the microsphere surface is facilitated by RGD modification of the alginate, making it suitable for cell carrying. Overall, the proposed easy-to-use technology enables fabrication of monodisperse and highly-sphered AMs by a simple microfabrication process, with no chance of microchannel clogging.

Data availability

The data supporting this article have been included within the article or as part of the ESI.†

Author contributions

Chen S. conceived the research, and Cohen S. supervised it. Chen S. designed and performed the experiments. Chen S., Cohen S., and Shahar T. contributed to the manuscript preparation. All authors approved the final version of the manuscript.

Conflicts of interest

There are no conflicts to declare.

Acknowledgements

This work was supported by the Avram and Stella Goldstein-Goren fund.

References

1 E. Ruvinov and S. Cohen, *Adv. Drug Delivery Rev.*, 2016, **96**, 54–76.
2 M. I. Neves, L. Moroni and C. C. Barrias, *Front. Bioeng. Biotechnol.*, 2020, **8**, 665.
3 M. B. Łabowska, I. Michalak and J. Detyna, *Open Chem.*, 2019, **17**, 738–762.
4 I. Berger Fridman, G. S. Ugolini, V. Vandelinder, S. Cohen and T. Konry, *Biofabrication*, 2021, **13**, 035037.
5 P. A. Dalavi, A. Prabhu, M. Sajida, K. Chatterjee and J. Venkatesan, *ACS Omega*, 2022, **7**, 26092–26106.
6 S. V. Shilova, G. M. Mirgaleev and V. P. Barabanov, *Polym. Sci., Ser. A*, 2022, **2022**, 1–9.
7 M. Chayosumrit, B. Tuch and K. Sidhu, *Biomaterials*, 2010, **31**, 505–514.
8 K. Y. Lee and D. J. Mooney, *Prog. Polym. Sci.*, 2012, **37**, 106.
9 Y. Sapir, O. Kryukov and S. Cohen, *Biomaterials*, 2011, **32**, 1838–1847.
10 Y. Sapir, B. Polyak and S. Cohen, *Nanotechnology*, 2013, **25**, 014009.
11 O. Tsur-Gang, E. Ruvinov, N. Landa, R. Holbova, M. S. Feinberg, J. Leor and S. Cohen, *Biomaterials*, 2009, **30**, 189–195.
12 B. F. Matlaga, L. P. Yasenchak and T. N. Salthouse, *J. Biomed. Mater. Res.*, 1976, **10**, 391–397.
13 J. C. De La Vega, P. Elischer, T. Schneider and U. O. Häfeli, *Nanomedicine*, 2013, **8**, 265–285.
14 L. Amirifar, M. Besanjideh, R. Nasiri, A. Shamloo, F. Nasrollahi, N. R. De Barros, E. Davoodi, A. Erdem, M. Mahmoodi, V. Hosseini, H. Montazerian, J. Jahangiry, M. A. Darabi, R. Haghniaz, M. R. Dokmeci, N. Annabi, S. Ahadian and A. Khademhosseini, *Biofabrication*, 2022, **14**, 022001.
15 M. Chen, G. Bolognesi and G. T. Vladisavljević, *Molecules*, 2021, **26**, 3752.
16 A. Sattari, S. Janfaza, M. Mashhadi Keshtiban, N. Tasnim, P. Hanafizadeh and M. Hoorfar, *ACS Omega*, 2021, **6**, 25964–25971.
17 Q. Q. Liao, S. K. Zhao, B. Cai, R. X. He, L. Rao, Y. Wu, S. S. Guo, Q. Y. Liu, W. Liu and X. Z. Zhao, *Sens. Actuators, A*, 2018, **279**, 313–320.
18 M. Samandari, F. Alipanah, S. Haghjooy Javanmard and A. Sanati-Nezhad, *Sens. Actuators, B*, 2019, **291**, 418–425.
19 H. Shieh, M. Saadatmand, M. Eskandari and D. Bastani, *Sci. Rep.*, 2021, **11**, 1–10.
20 A. Sattari, S. Janfaza, M. Mashhadi Keshtiban, N. Tasnim, P. Hanafizadeh and M. Hoorfar, *ACS Omega*, 2021, **6**, 25964–25971.
21 H. Ahmed and B. T. Stokke, *Lab Chip*, 2021, **21**, 2232–2243.
22 Y. Liu, N. Tottori and T. Nisisako, *Sens. Actuators, B*, 2019, **283**, 802–809.
23 L. Capretto, S. Mazzitelli, C. Balestra, A. Tosi and C. Nastruzzi, *Lab Chip*, 2008, **8**, 617–621.
24 M. G. Simon and A. P. Lee, *Microdroplet Technology – Principles and Emerging Applications in Biology and Chemistry*, 2012, pp. 23–50.
25 C. N. Baroud, F. Gallaire and R. Dangla, *Lab Chip*, 2010, **10**, 2032–2045.
26 S. Bäther, J. H. Seibt, C. S. Hundschell, J. C. Bonilla, M. P. Clausen and A. M. Wagemans, *Food Hydrocolloids*, 2024, **149**, 109538.
27 E. Rosellini, C. Cristallini, N. Barbani, G. Vozzi and P. Giusti, *J. Biomed. Mater. Res., Part A*, 2009, **91**, 447–453.
28 Y. S. Choi, S. R. Hong, Y. M. Lee, K. W. Song, M. H. Park and Y. S. Nam, *Biomaterials*, 1999, **20**, 409–417.
29 R. H. Tromp, A. R. Rennie and R. A. L. Jones, *Macromolecules*, 1995, **28**, 4129–4138.
30 Z. Dong, Q. Wang and Y. Du, *J. Membr. Sci.*, 2006, **280**, 37–44.
31 H. Huang, X. Qi, Y. Chen and Z. Wu, *Saudi Pharm. J.*, 2019, **27**, 990–999.
32 O. Tsur-Gang, E. Ruvinov, N. Landa, R. Holbova, M. S. Feinberg, J. Leor and S. Cohen, *Biomaterials*, 2009, **30**, 189–195.
33 J. P. Paques, E. Van Der Linden, L. M. C. Sagis and C. J. M. Van Rijn, *J. Agric. Food Chem.*, 2012, **60**, 8501–8509.
34 L. M. Kasankala, Y. Xue, Y. Weilong, S. D. Hong and Q. He, *Bioresour. Technol.*, 2007, **98**, 3338–3343.
35 P. Wu, Z. Luo, Z. Liu, Z. Li, C. Chen, L. Feng and L. He, *Chin. J. Chem. Eng.*, 2015, **23**, 7–14.
36 J. Xu, H. Fang, Y. Su, Y. Kang, D. Xu, Y. Y. Cheng, Y. Nie, H. Wang, T. Liu and K. Song, *Int. J. Biol. Macromol.*, 2022, **220**, 1253–1266.
37 I. Cicha, R. Detsch, R. Singh, S. Reakasame, C. Alexiou and A. R. Boccaccini, *Curr. Opin. Biomed. Eng.*, 2017, **2**, 83–89.
38 M. F. Butler and M. Heppenstall-Butler, *Food Hydrocolloids*, 2003, **17**, 815–830.
39 N. T. T. Uyen, Z. A. A. Hamid, N. X. T. Tram and N. Ahmad, *Int. J. Biol. Macromol.*, 2020, **153**, 1035–1046.
40 J. Rodness, A. Mihic, Y. Miyagi, J. Wu, R. D. Weisel and R. K. Li, *Acta Biomater.*, 2016, **45**, 169–181.
41 M. Grellier, P. L. Granja, J. C. Fricain, S. J. Bidarra, M. Renard, R. Bareille, C. Bourget, J. Amédée and M. A. Barbosa, *Biomaterials*, 2009, **30**, 3271–3278.